Dalton Transactions

ROYAL SOCIETY OF CHEMISTRY

PAPER

View Article Online
View Journal | View Issue

Cite this: *Dalton Trans.*, 2025, **54**, 12241

Impact of amorphization on the luminescence and UVC upconversion efficiency of $LaAlO_3:Pr^{3+}$ materials†

N. Miniajluk-Gaweł, *[a] A. Chudzyńska,[a,b] B. Bondzior, [a] N. Rebrova[a] and P. J. Dereń [a]

Received 27th May 2025,
Accepted 14th July 2025

DOI: 10.1039/d5dt01241d

rsc.li/dalton

In this work, we present a comparative study of $LaAlO_3:Pr^{3+}$ materials in both crystalline and amorphous specimens, exploring how structural differences influence their optical properties. Polycrystalline powders with a perovskite structure were synthesized *via* high-temperature solid-state reaction, and then transformed into spherical amorphous forms (~1 mm diameter) using the aerodynamic levitation method with CO_2 laser heating. Comprehensive structural (XRD, SEM, and EDS) and spectroscopic (emission, excitation, and decay time) analyses were performed. Particular focus was given to visible-to-ultraviolet upconversion in $LaAlO_3$:2% Pr^{3+} samples under 444 nm laser excitation. The study revealed distinct differences in luminescence behavior between the crystalline and amorphous phases, with the former showing enhanced upconversion efficiency. These results underline the critical role of local structural environments in tuning the photonic properties of Pr^{3+}-doped materials, offering valuable insights for the design of next-generation optical devices with applications in photonics, optoelectronics, and UV-based technologies.

Introduction

Praseodymium ions are well known for their ability to have optical transitions that enable them to be used in various fields such as optoelectronics, lasers and luminescent materials. In the case of Pr^{3+} ions present in an amorphous material, their spectroscopic properties, such as light absorption and emission, depend on the local structure of the surrounding matrix. These ions are particularly important in the context of luminescence properties resulting from their energy transitions of the of 4f–4f and 5d–4f types.[1] Electron transfer at these levels results in intense light emissions that can be tuned by modifying the deposition conditions and host structure. They are very well known for their fluorescence transitions in the visible range, starting from cyan, through green, orange and going up to deep red.[2] One of the interesting effects that can occur in materials with Pr^{3+} ions is the upconversion effect, which is a process in which two photons of lower energy are absorbed by a Pr^{3+} ion and then emitted as one photon of higher energy. This effect is particularly interesting in the context of optical materials, as it allows the creation of materials that can be excited with lower energy light and then emit higher energy light.[3,4]

There are quite a few literature reports regarding the luminescence properties of Pr^{3+} ions, in both single crystals and polycrystalline $LaAlO_3$ powder. Interesting results were obtained by one of us in ref. 5, in which the spectroscopic properties of the Pr^{3+} ion in the $LaAlO_3$ crystal were analyzed. It was shown that a single crystal exhibits a long $^3P_0$ lifetime, which does not depend on temperature, while the intensity of emission from the $^1D_2$ level does. The results obtained allowed us to state that the tested material is a promising laser system. Valuable results were presented in the paper,[6] where it was shown that by controlling the nanocrystallite size it is possible to tune the structure and thus the spectroscopic properties of the $LaAlO_3$ nanocrystals. These materials have been studied quite extensively in the field of thermoluminescence. The obtained results show that $LaAlO_3:Pr^{3+}$ can be used as a thermoluminescent material for diagnostic measurements of X-ray beams.[7–9] The properties of cathodoluminescence were also studied, with possible applications in the field of dosimetry or in devices emitting UV radiation.[10,11] A comparison between the luminescence efficiency of the same material in a crystalline and amorphous form containing Ln^{3+} ions is not new, as it has been carried out and published many years ago by George Blasse and his co-authors in the paper.[12] Nevertheless, to the best of our knowledge, no publications present the optical properties of $LaAlO_3$ doped with Pr^{3+} ions with amorphous structures, obtained by the aerodynamic levitation

[a]*Institute of Low Temperature and Structure Research, Polish Academy of Science, Okólna 2, 50-422 Wroclaw, Poland. E-mail: n.miniajluk@intibs.pl*
[b]*XTPL S.A., Stabłowicka 147, 54-066 Wroclaw, Poland*
† Electronic supplementary information (ESI) available. See DOI: https://doi.org/10.1039/d5dt01241d

method; therefore, the results presented in this paper are innovative.

In this work, we investigated the possibility of obtaining amorphous materials from polycrystalline $LaAlO_3$ perovskites doped with Pr^{3+}, by using an aerodynamic levitation method. This method was described in more detail in a paper about $LaAlO_3$:Tb^{3+} by some of the present authors.[13] This work focuses on the comparison of the structural and spectroscopic properties of $LaAlO_3$:Pr^{3+},both polycrystals obtained by solid-state reaction and amorphous materials obtained by aerodynamic levitation.

The purpose of this publication is to study in detail the effect of doping with Pr^{3+} ions on the structural and spectroscopic properties of amorphous $LaAlO_3$ materials. Also, the studies conducted on these materials are focused on the upconversion properties. In amorphous materials, where Pr^{3+} ions are distributed more randomly, upconversion can occur, but with varying efficiency depending on the local structural properties of the surrounding matrix. The results of the research may contribute to the development of new functional materials for use in innovative optoelectronic and luminescent devices. Furthermore, this work opens up promising prospects for the practical use of $LaAlO_3$:Pr^{3+} in disinfection and sterilization technologies.

Experimental

Sample preparation

A series of polycrystalline powders with a single perovskite structure $LaAlO_3$ were obtained by a conventional high-temperature solid-state method. La_2O_3, Al_2O_3, and Pr_6O_{11} were used as raw materials. The stoichiometric amount of oxides according to the chemical formula $La_{1-x}Pr_xAlO_3$ (x = 0.1, 0.25, 0.5, 1, 2, 5 mol%) was thoroughly mixed in an agate mortar with absolute ethanol. The homogeneous powders were dried at 70 °C for 24 h and calcined at 800 °C for 12 h and then at 1500 °C for 5 h.

We used the aerodynamic levitation method with a CO_2 laser to convert the obtained polycrystalline powders into amorphous structures in the form of spheres with diameters around 1–2 mm. The process involved pre-melting the powder with a CO_2 laser to form a spherical structure. The temperature of the sample was kept above the melting point for several seconds to ensure homogenization of the melt. The sample was then levitated in a nitrogen stream with the flow rate set around 500 ml min^{-1} and was completely melted by the CO_2 laser. After turning off the laser power, the sample was rapidly cooled to room temperature resulting in the formation of amorphous beads with a diameter of 2 mm. For further microstructural studies, the surfaces of the obtained structures were ground and polished to obtain a flat surface.

Research techniques

X-ray diffraction (XRD) patterns were recorded with an X'Pert ProPANalytical X-ray diffractometer, working in the reflection geometry, using Cu Kα radiation (λ = 1.54056 Å). The data were collected in a 2Θ range from 10° to 90° with a step of 0.026°.

A scanning electron microscope (FEI NOVA NanoSEM 230, equipped with an EDAX Genesis XM4 detector) was used to characterize the morphology and chemical composition of the samples with an accelerating voltage of 20 kV. The SEM images were recorded with an accelerating voltage of 5 kV.

Emission and excitation spectra and decay curves were obtained by using an FLS1000 Edinburgh Instruments spectrophotometer in a Czerny–Turner configuration with VIS and NIR detectors at room temperature. The light sources used in this system are a micro-second pulse lamp and a 450 W xenon lamp.

The upconversion luminescence of the samples was recorded using a McPherson Model 218 scanning monochromator with continuous laser excitation at a wavelength of 444 nm. The laser beam was focused into a rectangular spot (1 mm × 1.5 mm) using a lens with a focal length of 20 cm. To measure the upconversion lifetime, the second harmonic of a Ti:sapphire laser, pumped by the second harmonic of a Nd:YAG laser (LOTIS TII, Belarus), was employed as a pulsed excitation source. A UG5 optical filter and a solar-blind photomultiplier (Hamamatsu R7154P) were used to measure the upconversion characteristics.

Results and discussion

$LaAlO_3$ powders doped with Pr^{3+} were characterized by X-ray powder diffraction (XRD). The obtained XRD patterns of polycrystalline powders are presented in Fig. 1, compared to the reference standard card for the regular structure of $LaAlO_3$ (ICDD 96-220-6577). The materials are well-crystallized; the observed peaks are sharp and well-defined. The obtained polycrystalline powders are single-phase. Fig. S1† shows XRD patterns after the melting of $LaAlO_3$:Pr^{3+} powders by using the

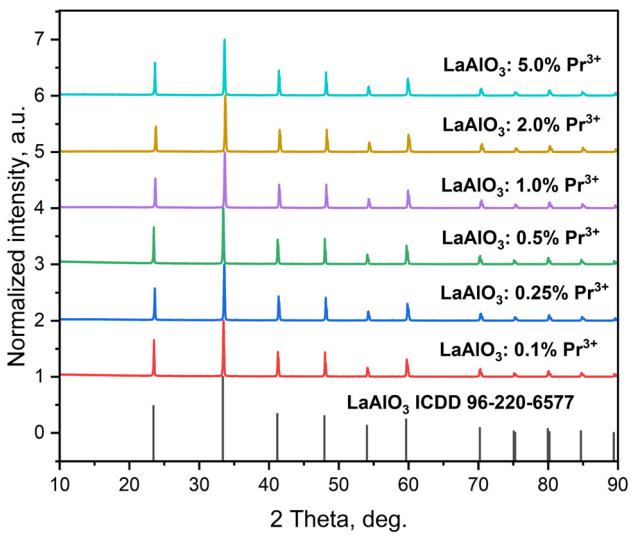

Fig. 1 XRD patterns of $LaAlO_3$:Pr^{3+} polycrystalline powders.

aerodynamic levitation method. The resulting samples are completely amorphous, as indicated by the lack of Bragg peaks in the XRD pattern.

Fig. 2a shows the SEM image of polycrystalline $LaAlO_3:Pr^{3+}$ powders with a histogram of the average crystal size. The material consists of crystallites with undefined shapes, varying in size from 0.2 to 0.8 μm. These crystallites tend to agglomerate. Fig. 2b shows the SEM image and linear energy-dispersive X-ray spectroscopy (EDS) analysis of the cross-section of the amorphous $LaAlO_3:Pr^{3+}$ sample. EDS results prove that the aerodynamic levitation method successfully formed an amorphous material with full homogeneity and no structural defects. The ions are homogeneously distributed across the entire surface.

The emission spectra of polycrystalline powders and amorphous materials, presented in Fig. 3, were obtained with excitation at 447 nm and measured at room temperature (300 K). In the obtained emission spectra for polycrystalline powders (Fig. 3a), a strong blue emission is visible. The most intense emission band was obtained for the $^3P_0 \rightarrow {}^3H_4$ transition at 491 nm, which is complemented by smaller maxima in the green region for $^3P_1 \rightarrow {}^3H_5$ (523 nm) and in the orange region for $^1D_2 \rightarrow {}^3H_4$ (612 nm). The entire spectrum of emissions is complemented by transitions from $^3P_0$ to $^3F_2$, $^3F_3$ and $^3F_4$. All these transitions are associated with emission in the red range and contribute to the broadening of the emission spectrum in the polycrystalline powder $LaAlO_3:Pr^{3+}$. From the presented polycrystalline powder emission characteristics, the optimal concentration of praseodymium ions is 2 mol%. Amorphous materials obtained by aerodynamic levitation exhibit broadband emission (Fig. 3b). The transitions with the highest intensity are for concentration of Pr^{3+} = 1 mol%, mainly from $^3P_0$ to $^3H_4$, $^3H_6$ and $^3F_2$ and then a significant decrease in the emission efficiency of amorphous materials caused by concentration quenching was observed. The full width at half maximum (FWHM) values for the $^3P_0 \rightarrow {}^3H_4$ transition were determined for both powders and amorphous materials and are: 75 cm^{-1} and 982 cm^{-1}, respectively. For amorphous structures, the FWHM value is much higher, because due to the structural disorder the emission peaks are broadened.[14]

Fig. 4 illustrates the excitation spectrum of polycrystalline powders and amorphous structures. Emission was monitored

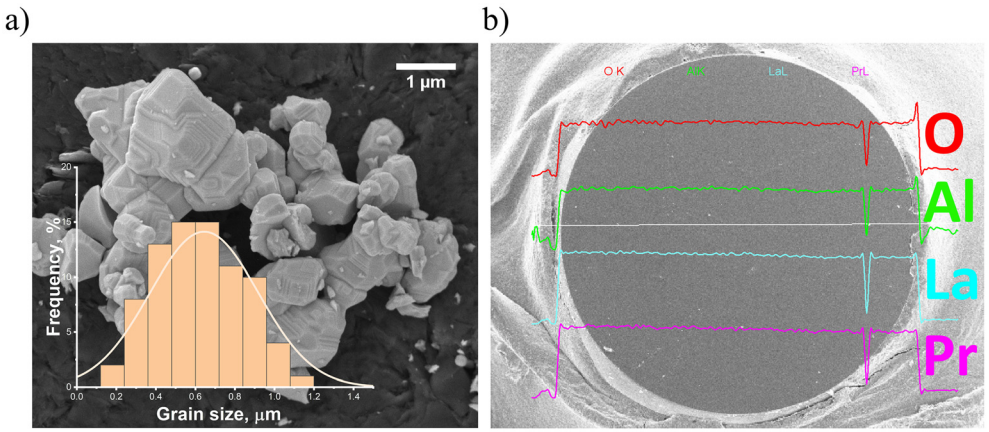

Fig. 2 $LaAlO_3:Pr^{3+}$: (a) SEM images of powders prepared by the solid state method and (b) SEM with the EDS spectrum of amorphous structures prepared by the aerodynamic levitation method.

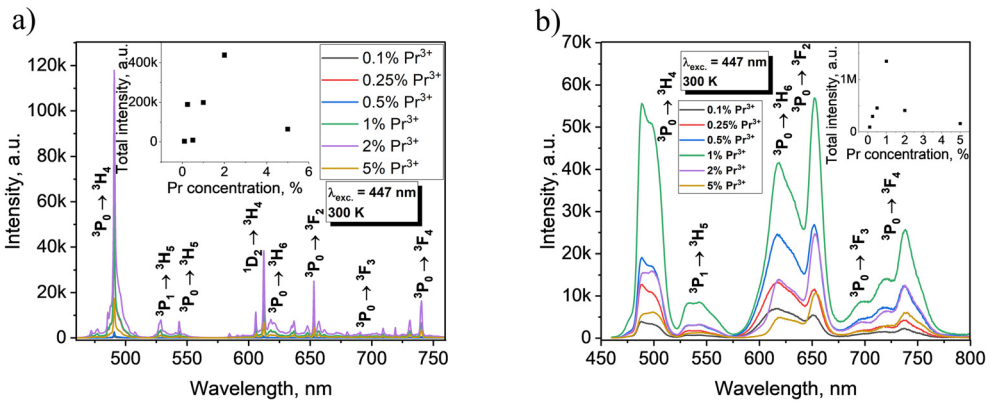

Fig. 3 Emission spectrum of $LaAlO_3:Pr^{3+}$ with an excitation wavelength of 447 nm of (a) polycrystalline powders and (b) amorphous materials.

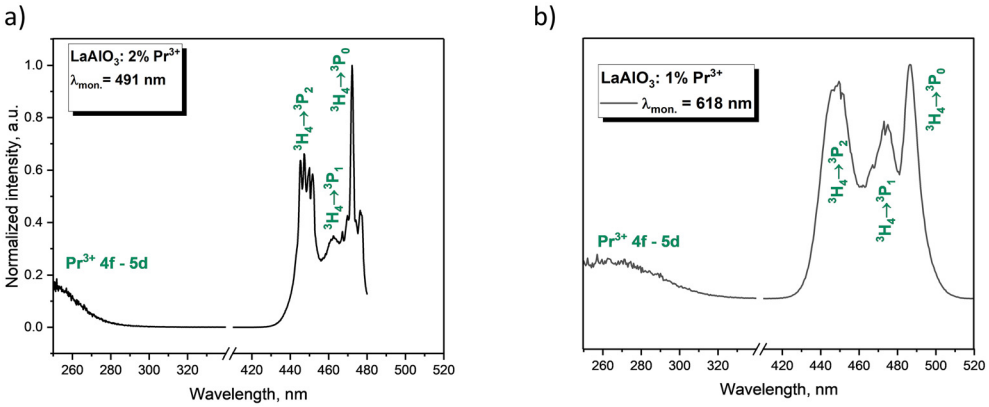

Fig. 4 $LaAlO_3$:Pr^{3+} excitation spectrum of (a) polycrystalline powders and (b) amorphous materials.

at 491 nm for powders, while for amorphous materials, emission was monitored at 618 nm. Measurements at both of these wavelengths were chosen to obtain a comprehensive picture of the emission spectra of amorphous materials, considering the different energy transitions of Pr^{3+} ions. In the case of powder emission (Fig. 4a), we observed well-distinguishable bands corresponding to transitions from the ground level $^3H_4$ to the excited levels $^3P_0$, $^3P_1$, and $^3P_2$, with maxima at 472 nm, 462 nm, and 447 nm, respectively. As for the spectroscopic properties of amorphous $LaAlO_3$:Pr^{3+} (Fig. 4b), the excitation spectrum is quite similar to that recorded for polycrystalline samples; however, several differences are noticeable. The first is the increased intensity of the transition lines, especially for the excitation to the $^3P_1$ and $^3P_2$ levels. Another noticeable difference is the change in the excitation lines; the FWHM of the glass sample is wider and slightly shifted. According to literature reports, the broad band at about 260 nm was assigned to the 4f → 5d transition of the Pr^{3+} ions, respectively, for polycrystalline powders and amorphous samples.[15]

Luminescence decay curves of polycrystalline powders doped with Pr^{3+} are single-exponential at a low concentration of Pr^{3+} (see Fig. 5a), which suggests that the Pr^{3+} dopant occupies a single crystallographic site, replacing the La^{3+} ion. At low concentrations of Pr^{3+}, the lifetime of $^3P_0$ was equal to 30.5 μs, which is a typical value for crystalline $LaAlO_3$.[3] At low concentration of Pr^{3+}, the decay times are longer because the praseodymium ions are less likely to interact with each other, allowing for efficient emission. However, higher concentrations of Pr^{3+} ions lead to a phenomenon known as luminescence quenching. This effect becomes particularly pronounced at concentrations above 2 mol%, where the decays occur rapidly faster (see Fig. 5a inset). The Inokuti–Hirayama model[16] was implemented to estimate the critical radius for energy transfer responsible for concentration quenching. The decay curves were fitted with the following eqn (1)

$$I(t) = I_0 \exp\left(\frac{-t}{\tau_r} - \alpha\left(\frac{t}{\tau_r}\right)^{\frac{3}{s}}\right) \quad (1)$$

$$\alpha = \frac{4}{3}\pi\Gamma\left(1 - \frac{3}{s}\right) n_A {R_0}^3 \quad (2)$$

where I_0 is the initial intensity after the excitation pulse, τ_R is the radiative lifetime, s is the multipolar interaction parameter equal to 6, 8 or 10 for dipole–dipole, dipole–quadrupole and quadrupole–quadrupole interactions. n_A is the number of dopant ions per volume unit and R_0 is the critical radius. From the slope of the α parameter over n_A, the critical radius for crystalline $LaAlO_3$:Pr was determined to be 7.69 Å. The model fitted the best for s equal to 6, which means the mechanism of ionic interactions is dipole–dipole interactions. Based on a previous report on Pr^{3+} concentration quenching, the mechanism of excited level depopulation is a $(^3P_0, ^3H_4) \rightarrow (^1D_2, ^3H_6)$ cross-relaxation,[17] which is consistent with the dipole–dipole interaction mechanism.[18]

Luminescence decay curves of glass samples exhibit substantially faster decay (see Fig. 5c). For low concentrations of Pr^{3+}, the decay time of the $^3P_0$ level is only 8.2 μs. For higher concentrations, the decay time undergoes a similar concentration quenching process as polycrystalline samples. The Inokuti–Hirayama model was used analogically to determine the critical radius for energy transfer between Pr^{3+} ions. The model was used with assumptions of equal density of crystalline and glassy $LaAlO_3$, due to an inability to accurately measure the density of tiny ball samples. The critical radius was determined to be only slightly smaller than that of crystalline $LaAlO_3$ and equal to 7.07 Å. The mechanism for ionic interactions was also dipole–dipole interactions. The obtained result is important because it indicates that the transformation from the crystalline to amorphous $LaAlO_3$ does affect the transitions rates of the Pr^{3+} dopant but does not significantly affect the interionic interactions.

Pr^{3+} is an ideal candidate for ultraviolet upconversion luminescence because its intermediate ^3P_J levels can be easily excited by violet and blue lasers (430–490 nm) and then in the next step they can reach the 5d4f level through several mechanisms, like excited-state absorption (ESA) and energy transfer upconversion (ETU) for example.[19] In the ESA mechanism, a praseodymium ion sequentially absorbs two photons, transi-

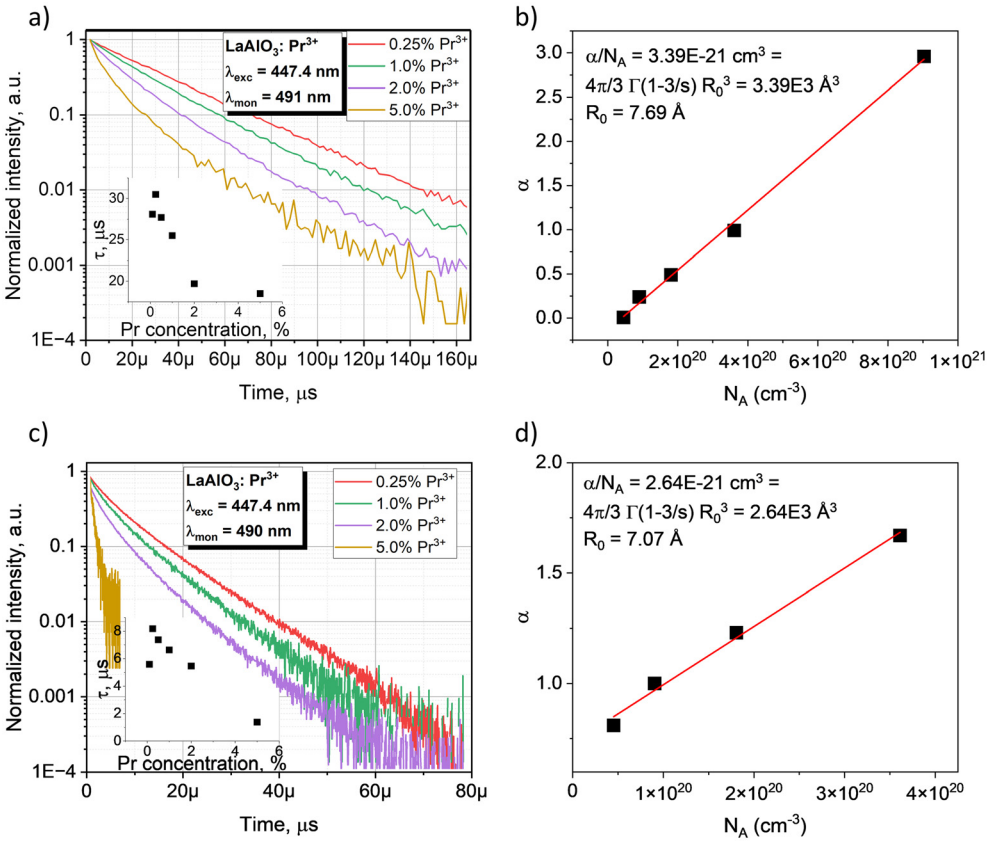

Fig. 5 $LaAlO_3$:Pr^{3+} decay curves of the $^3P_0$ emission of polycrystalline powders (a) and $LaAlO_3$ amorphous materials (c). Relevant fitting according to the Inokuti–Hirayama model is shown as well for polycrystalline (b) and amorphous materials (d).

tioning from the ground state to the 5d–4f level *via* the ^3P_J states (or the $^1D_2$ state in certain matrices), without involving energy transfer. In contrast, the ETU mechanism involves a pair of neighboring Pr^{3+} ions – one ion acting as a sensitizer and the other as an activator. The second ion is promoted to the 4f5d state, from which upconversion emission occurs.[19] Depending on the band gap, upconversion radiation due to the $5d^14f^1 \rightarrow 4f^2$ transition of the Pr^{3+} ion can be observed in the UV-C, UV-B and UV-A ranges.[20,21] Fig. 6a shows upconverted emission of the $LaAlO_3$:2%Pr^{3+} powder sample and amorphous materials, under 444 nm excitation. The upconversion emission of the powder sample is significantly stronger than that for the amorphous one. This difference can be explained by several factors. First, there are many praseodymium ion sites in the amorphous materials, between which energy transfer occurs. Second, Z. Yin *et al.*[22] suggest that in transparent amorphous materials, only Pr^{3+} ions located directly in the light path are excited. In contrast, in the ceramic material, the excitation light is scattered, increasing its optical path and providing excitation of Pr^{3+} ions outside the direct light path, which contributes to an increase in upconversion intensity. The presence of upconversion emission highlights the potential of the powder sample for surface sterilization, particularly when applied as a thin film.[23]

During the upconversion process, the emission intensity (I) and laser pump power (P) follow the relationship $I \propto P^n$, where n is the number of photons required to populate the upconversion energy level.[24] The corresponding logarithmic dependence is presented in the inset of Fig. 6b. The linear approximation of the experimental data gives a slope of 1.7. This indicates that the ultraviolet emission is the result of a two-photon upconversion process, which in praseodymium-activated inorganic compounds can occur either through excited-state absorption or energy-transfer upconversion. To identify the mechanism under pulsed laser excitation, the upconversion lifetime of a $LaAlO_3$:2%Pr^{3+} powder sample was measured under 444 nm pulsed laser excitation (Fig. 6b). The upconversion emission decay profile exhibits a hump around 180 ns, known as ringing, which often occurs when measuring very short pulses with an oscilloscope.[25,26] The decay curve was fitted using a biexponential function (3):

$$I(t) = A_1 \exp\left(-\frac{t}{\tau_1}\right) + A_2 \exp\left(-\frac{t}{\tau_2}\right) \quad (3)$$

where A_1 and A_2 represent the amplitudes of each decay component and τ_1 and τ_2 are the lifetimes. A biexponential fit yields decay constants of about 17.6 and 209 ns. The main component

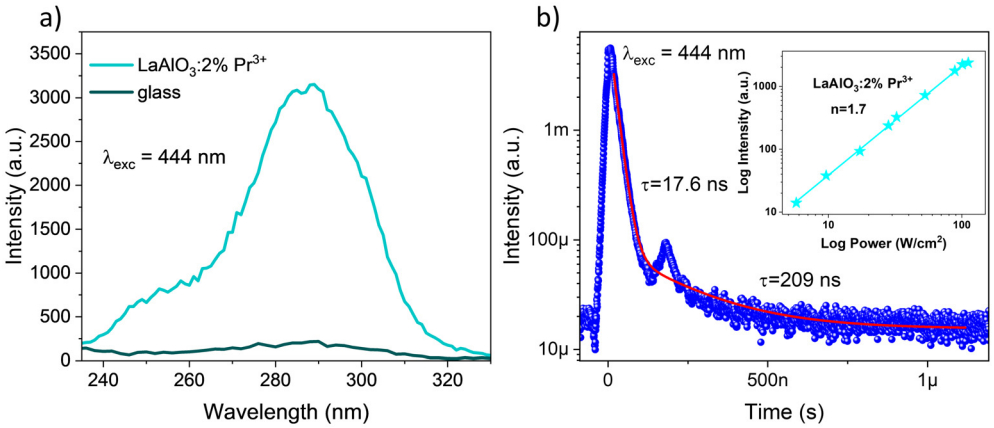

Fig. 6 (a) Upconversion spectra of the amorphous materials and $LaAlO_3$:2%Pr^{3+} powder sample under 444 nm continuous wavelength laser excitation at room temperature, (b) decay of upconversion emission under 444 nm pulsed excitation of the $LaAlO_3$:2%Pr^{3+} powder sample. Inset: the relationship between the excitation power of a 444 nm laser and the resulting emission intensity at 288 nm.

of 17.6 ns (99.2% of whole decay) is attributed to $5d^14f^1 \rightarrow 4f^2$ Pr^{3+} radiation, while the presence of a long component (0.8%) is associated by Schröder *et al.*[27] to the participation of luminescent defects. It is known from the literature that for praseodymium-activated matrices, the upconversion lifetime of the ESA mechanism equals the $5d^14f^1 \rightarrow 4f^2$ emission lifetime of the Pr^{3+} ion, which is on the order of tens of nanoseconds.[28] Thus, this mechanism is responsible for upconversion in the $LaAlO_3$:Pr^{3+} powder sample in the case of pulsed excitation.

The thermal stability of luminescence was evaluated for polycrystalline (Fig. S2a†) and amorphous materials (Fig. S2b†). The amorphous sample exhibits slightly reduced luminescence intensity with the increase in temperature compared to the polycrystalline sample (Fig. S2c†), but their activation energy determined from the Arrhenius equation is comparable (Fig. S2d†) and equal to ~350 cm^{-1}.

While crystalline $LaAlO_3$:Pr exhibits superior ultraviolet upconversion ability, amorphous $LaAlO_3$:Pr can be used as a

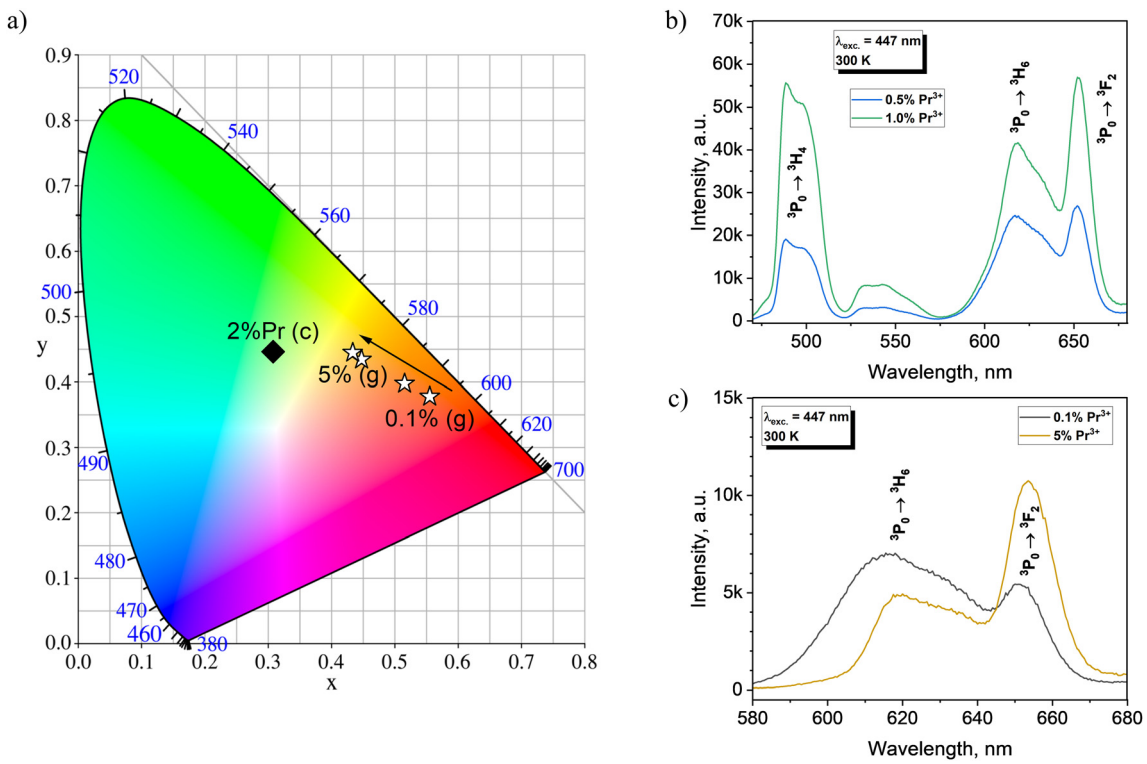

Fig. 7 (a) CIE color coordinates of $LaAlO_3$:Pr powder (c) and amorphous materials samples (g), (b) visible region of the $LaAlO_3$:Pr (0.5% and 1%) glass emission spectrum, and (c) red region of the $LaAlO_3$:Pr (0.1% and 5%) amorphous material emission spectrum.

red-orange phosphor due to its broad emission bands and tunable color. Fig. 7a illustrates the CIE color coordinates of the crystalline and amorphous materials. While the emission from the crystalline $LaAlO_3$:Pr is mostly green, with CIE coordinates of $x = 0.306$ and $y = 0.448$, and the shape of the emission spectrum does not change with Pr^{3+} concentration, the amorphous materials exhibit color coordinates from orange-red for 0.1% Pr^{3+} ($x = 0.553$, $y = 0.380$) to yellow for 5% Pr^{3+} ($x = 0.432$, $y = 0.447$). The tunability of the emission manifests itself in the shift in the blue-green to red ratio – samples with higher Pr^{3+} concentration tend to emit a stronger blue-green $^3P_0 \rightarrow {}^3H_4$ transition at 491 nm (see Fig. 7b), as well as different 655 nm to 620 nm ratios, which also tend to increase for higher Pr^{3+} concentration (see Fig. 7c). These shifts in emission band ratios are not uncommon for non-crystalline materials with changing chemical compositions, where dopant ions act as network modifiers and induce changes in the branching ratios of lanthanide emission.[29–32]

Conclusions

In this study, we successfully synthesized $LaAlO_3$:Pr^{3+} polycrystalline powders and transformed them into amorphous spherical specimens using the aerodynamic levitation method. Comparative analysis revealed clear differences in structural and spectroscopic properties between the crystalline and amorphous forms. While the crystalline powders exhibited strong visible-range luminescence, the amorphous materials showed broadened emission bands with concentration-dependent quenching. Notably, the upconversion properties under 444 nm excitation highlighted the superior UV emission performance of the crystalline form, attributed to enhanced photon scattering and excitation efficiency. These findings confirm the significant influence of the host structure on the optical behavior of Pr^{3+} ions and open up promising applications in UV-emitting optoelectronic and sterilization devices. From the Inokuti–Hirayama model, it was found that the transformation of $LaAlO_3$ from the crystalline to amorphous state affects the transition rates of the Pr^{3+} dopant but does not significantly affect the interionic interactions.

Conflicts of interest

There are no conflicts do declare.

Data availability

Data will be made available on request.

Acknowledgements

We want to thank INTiBS PAN for its financial support in the framework of statutory activities (task 2018/19).

References

1 M. Malinowski, M. Kaczkan, S. Turczynski and D. Pawlak, *Opt. Mater.*, 2011, **33**, 1004–1007.
2 F. Reichert, F. Moglia, D.-T. Marzahl, P. Metz, M. Fechner, N.-O. Hansen and G. Huber, *Opt. Express*, 2012, **20**, 20387–20395.
3 X. Zhou, J. Qiao, Y. Zhao, K. Han and Z. Xia, *Sci. China Mater.*, 2022, **65**(4), 1103–1111.
4 X. Zhou, L. Ning, J. Qiao, Y. Zhao, P. Xiong and Z. Xia, *Nat. Commun.*, 2022, **13**, 7589.
5 P. J. Dereń, Spectroscopic characterization of $LaAlO_3$ crystal doped with Pr^{3+} ions, *J. Lumin.*, 2007, **122–123**, 40–43.
6 P. J. Dereń and K. Lemański, On tuning the spectroscopic properties of $LaAlO_3$:Pr^{3+} nanocrystallites, *J. Lumin.*, 2011, **131**, 445–448.
7 N. Vazquez-Flores, E. R. Vázquez-Cerón, M. Osorio-Valero, D. Nolasco-Altamirano, A. A. Barrera-Angeles and T. Rivera-Montalvo, *J. Phys.: Conf. Ser.*, 2022, **2307**, 012046.
8 M. A. de León-Alfaro, A. Morales-Hernández, J. Roman-Lopez, J. Zarate-Medina and T. Rivera-Montalvo, *Appl. Radiat. Isot.*, 2018, **132**, 57–60.
9 T. Rivera-Montalvo, A. Morales-Hernandez, A. A. Barrera-Angeles, R. Alvarez-Romero, C. Falcony and J. Zarate-Medina, *Radiat. Phys. Chem.*, 2017, **140**, 68–73.
10 C. Boronat, T. Rivera, J. Garcia-Guinea and V. Correcher, *Radiat. Phys. Chem.*, 2017, **130**, 236–242.
11 Y. Shimizu, K. Ueda, H. Takashima and Y. Inaguma, *Phys. Status Solidi A*, 2015, **212**, 703–706.
12 J. W. M. Verwey, D. Van Der Voort, G. J. Dirksen and G. Blasse, *J. Solid State Chem.*, 1990, **89**, 106–117.
13 N. Miniajluk-Gaweł, B. Bondzior, A. Chudzyńska and P. J. Dereń, *J. Alloys Compd.*, 2025, **1010**(5), 177088.
14 B. Bondzior, C. Nguyen, T. H. Q. Vu, P. J. Dereń and L. Petit, *Mater. Chem. Phys.*, 2024, **311**, 128493.
15 Y. Shimizu, Y. Takano and K. Ueda, *Thin Solid Films*, 2014, **559**, 23–26.
16 M. Inokuti and F. Hirayama, *J. Chem. Phys.*, 1965, **43**, 1978–1989.
17 Y. Kitagawa, H. Nakamura and K. Shinozaki, *J. Mater. Chem. C*, 2024, **12**, 18865–18876.
18 S. Hau, C. Gheorghe, L. Gheorghe, F. Voicu, M. Greculeasa, G. Stanciu, A. Broasca and M. Enculescu, *J. Alloys Compd.*, 2019, **799**, 288–301.
19 F. Auzel, *Chem. Rev.*, 2004, **104**, 139–174.
20 Y. Kitagawa, H. Nakamura and K. Shinozaki, *J. Mater. Chem. C*, 2024, **12**, 18865–18876.
21 E. L. Cates, A. P. Wilkinson and J. H. Kim, *J. Lumin.*, 2015, **160**, 202–209.
22 Z. Yin, Z. Zhu, P. Lv, X. Zhang, X. Qi and Y. Yang, *Mater. Lett.*, 2021, **291**, 129613.
23 X. Zhao, F. Liu, T. Shi, H. Wu, L. Zhang, J. Zhang, X. J. Wang and Y. Liu, *Adv. Photonics Res.*, 2022, **3**, 2200106.
24 E. L. Cates and J. H. Kim, *Opt. Mater.*, 2013, **35**, 2347–2351.
25 N. Rebrova, P. Zdeb and P. J. Dereń, *J. Phys. Chem. C*, 2024, **128**, 9090–9098.

26 F. Lai, X. Xu, J. Shen, Y. Wang, Y. Yan, Y. Nie, W. You, D. Wu, L. Han and Z. Xiao, *Springer Nat.*, 2023, **15**, 1913–1923.
27 F. Schröder, S. Fischer and T. Jüstel, *Aust. J. Chem.*, 2022, **75**, 760–771.
28 N. Rebrova, A. Grippa, P. Zdeb and P. J. Dereń, *Scr. Mater.*, 2025, **255**, 116395.
29 H. Ebendorff-Heidepriem, D. Ehrt, M. Bettinelli and A. Speghini, *J. Non-Cryst. Solids*, 1998, **240**, 66–78.
30 P. Lopez-Iscoa, *et al.*, *J. Non-Cryst. Solids*, 2017, **460**, 161–168.
31 B. Bondzior, C. Nguyen, T. H. Q. Vu, D. Pugliese, P. J. Dereń and L. Petit, *J. Lumin.*, 2022, **252**, 119386.
32 B. Glorieux, T. Salminen, J. Massera, M. Lastusaari and L. Petit, *J. Non-Cryst. Solids*, 2018, **482**, 46–51.